Energy Technology
Generation, Conversion, Storage, Distribution
www.entechnol.de

Gravure-Printed Conversion/Alloying Anodes for Lithium-Ion Batteries

Maria Montanino, Giuliano Sico, Anna De Girolamo Del Mauro, Jakob Asenbauer, Joachim R. Binder, Dominic Bresser,* and Stefano Passerini*

Recently, printing techniques are increasingly investigated in the field of energy storage, especially for the fabrication of custom-designed batteries. Thanks to its many advantages, the most industrially used gravure printing would offer an innovative boost to printed battery production, even if, to date, such a technique is still not well investigated. In this study, for the first time, gravure printing is successfully used to prepare high-performance conversion/alloying anodes for lithium-ion batteries. A multilayer approach allows obtainment of the desired mass loading (about 1.7 mg cm^{-2}), reaching similar mass loadings to those obtained by commonly used lab-scale tape-casting methods, allowing for their comparison. High-quality gravure-printed layers are obtained showing a very high homogeneity, resulting in a high reproducibility of their electrochemical performance, very close to the theoretical value, and a long cycle life (up to 400 cycles). The good results are also due to the ink preparation method, using a ball-milling mix of the powders for disaggregation and homogenization of the starting materials. This work demonstrates the possibility of using the highly scalable gravure printing not only in the industrial manufacturing of printed batteries, but also as a useful tool for the study of new materials.

1. Introduction

Printed battery cells, having a volume below 10 mm^3 and a specific capacity in the range of 5–10 mAh cm^{-2}, are increasingly investigated for their use in portable electronics.[1] Recently, a lot of progress has been made in this field in terms of optimization of materials and processes.[2–8] The field is expected to further increase because certain novel devices, such as wearable electronics, biomedicine, and the Internet of Things require integrated thin and custom-designed batteries.[9] To date, the few industrially produced printed batteries are mostly primary, i.e., nonrechargeable cells.[1] Considering the different printing techniques available, gravure printing appears particularly attractive because it combines high-quality and high-speed production and the potential for scale-up to large production volumes.[10,11] Such a roll-to-roll printing technique, which is widely used for printing magazines and flexible packaging, may allow the manufacturing of low-cost and flexible structures and devices with high throughput. Gravure printing is a direct one-step deposition process at ambient conditions, suitable for large-area production and customized shapes, providing limited waste of energy, time, and materials.[12–16] Despite its many advantages, there are only a few studies on gravure printing, especially for the production of rechargeable lithium-ion batteries (LIBs), which instead are more and more investigated, including the search for cheaper production methods.[17–19] In the last years, we explored the possibility to gravure print layers of different functional materials, such as polymers and ceramics, for various technological purposes.[20–24] More recently, we successfully fabricated positive electrodes (cathodes) for LIBs by gravure printing, obtaining high performance and reproducibility as well as long cycle life.[25] These preliminary results demonstrate that gravure printing of electrodes and, in perspective, full cells (multiple-layer printing) can be potentially useful for industrial production. Moreover, thanks to the achievable high quality of the gravure-printed layer, the technique can be also considered a very versatile tool for the study and development of new battery materials because the deposition technique largely influences their performance.

To date, the feasible application of gravure printing for high-capacity negative electrodes (anodes) for LIBs has not been

M. Montanino, G. Sico, A. De Girolamo Del Mauro
Italian National Agency for New Technologies
Energy and Sustainable Economic Development (ENEA)
Portici Research Centre
Portici, Naples I-80055, Italy
E-mail: maria.montanino@enea.it

J. Asenbauer, D. Bresser, S. Passerini
Helmholtz Institute Ulm (HIU)
Ulm 89081, Germany
E-mail: dominic.bresser@kit.edu

J. Asenbauer, D. Bresser, S. Passerini
Karlsruhe Institute of Technology (KIT)
Karlsruhe 76021, Germany

J. R. Binder
Institute for Applied Materials
Karlsruhe Institute of Technology
Eggenstein-Leopoldshafen, Karlsruhe 76344, Germany

The ORCID identification number(s) for the author(s) of this article can be found under https://doi.org/10.1002/ente.202100315.

DOI: 10.1002/ente.202100315

exploited. In this work, we use carbon-coated $Zn_{0.9}Fe_{0.1}O$ ($Zn_{0.9}Fe_{0.1}O$–C) as a reference conversion/alloying material (CAM) to produce electrodes by gravure printing.[26] CAMs are a relatively new class of high-performance Li-ion anodes.[27] The idea of CAMs is to synergistically combine the conversion and alloying mechanism in one single material to overcome the general challenges of these two mechanisms, i.e., the large voltage hysteresis observed for conversion-type compounds and the extensive volume variations upon de-/lithiation in the case of alloying-type compounds,[28–30] while benefitting from their advantages, i.e., the fast de-/lithiation kinetics of conversion materials and the low de-/lithiation potential and limited voltage hysteresis of alloying materials.[27] This has been recently investigated amongst others for the herein studied $Zn_{0.9}Fe_{0.1}O$–C, which shows a high specific capacity, good rate capability, and good cycle life.[31,32] Furthermore, it is environmentally-friendly and consists of rather cheap and abundant elements. Moreover, in an attempt to keep the green aspects of the process and components, according to the most recent research,[33,34] the gravure-printed anodes were prepared using a water-soluble binder and deposited by water-based inks. Thanks to the herein pursued multilayer approach, it was possible to produce gravure-printed anodes with a similar mass loading to that commonly produced by lab-scale tape casting, allowing a possible comparison of the anodes produced by both the techniques.

2. Results and Discussion

The herein used CAM, $Zn_{0.9}Fe_{0.1}O$–C, is composed of environmentally-friendly and abundant elements. It has been shown to possess good characteristics for application in batteries, namely, a high specific capacity (theoretically: 966 mAh g^{-1}) and very good rate capability.[26] The reaction mechanism is based on the reversible conversion reaction, leading to the formation of metallic nanograins of Zn^0, Fe^0, and a Zn_xFe alloy (with $x > 1$) and the reversible alloying reaction of Zn^0 and Zn_xFe with lithium.[35]

Here, the gravure printing was used to prepare anodes for LiBs based on such a CAM as the active material. In the gravure printing process, a low-viscosity ink (1–100 mPa s) is directly transferred from the microengraved cells of a printing cylinder onto a flexible substrate by the pressure of a rubber cylinder, as shown in **Figure 1**.[10,36] The quality of the final printed layer depends on several physical parameters of the ink (viscosity, rheological behavior, surface tension, solvent evaporation rate), of the substrate (surface energy, porosity, smoothness), and of the process (i.e., cell geometry and density, printing pressure, speed).[16,24,37] The gravure printing process can be described as a sequence of subprocesses, concurring to the final material arrangement in the printed layer: The microengraved cells on the cylinder are filled with ink (*inking*); a blade removes the excessive ink from the cylinder (*doctoring*); the ink is transferred onto the substrate by the pressure of a counter cylinder (*transfer*); single droplets of the ink coalesce on the substrate, forming a continuous film (*spreading*); and the solvent is removed from the film, causing the final arrangement of the layer (*drying*).[24] Because of its complex, multiphysical nature, dimensional analysis is typically used for representing the physical system during each stage of the gravure printing process. Essentially, the fluid-dynamics of the process are determined by the balance between viscosity and surface tension forces, where the latter are the driving forces. Their balance can be described, at a fixed printing speed (U), by the dimensionless capillary number $Ca = \eta U/\gamma$, where η and γ are the viscosity and the surface tension of the ink, respectively.[10,24] The different subprocesses of gravure can have different dependencies on Ca, thus generating different regimes. At low Ca values, the pattern fidelity can be worsened by the ink drag-out from the microcells, whereas, at high Ca, ineffective doctoring leaves the ink in the nonprinted areas. Typically, good printing quality can be obtained by adjusting the ink parameters and the print speed to achieve a $Ca \approx 1$.[16] However, since the final print quality depends on the interplay of all the involved parameters, the optimal regime can be achieved by properly shifting the Ca to more favorable values.[10]

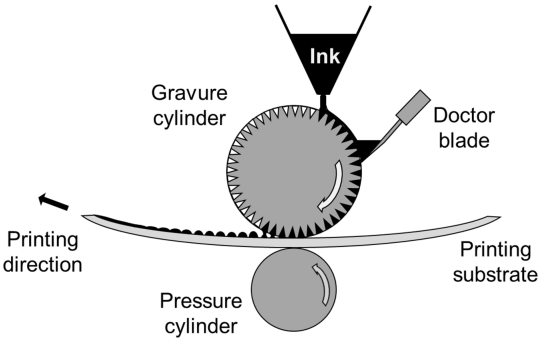

Figure 1. Schematic illustration of the gravure printing process.

To date, the difficulty in making composite electrodes with appropriate mass loading for commercial LIBs, due to the low ink viscosity, has limited the application of gravure printing to the field of batteries, while the electrodes are typically tape cast using high-solid-content slurries.[38,39] As the gravure printing requires large amounts of solvent, water was chosen as the prevalent solvent thanks to the use of water-based binders, improving the printing process sustainability. The solvent plays a key role in the printing process because it controls the surface tension and viscosity of the ink, on which the gravure printing fluid dynamics critically depend. In particular, the surface tension of the ink must be lower than the surface energies of the microengraved chrome-plated cylinder (42 mN m^{-1}) and of the substrate to properly wet them, allowing an efficient printed ink-to-cell volume ratio. For this purpose, Corona pretreatment of the substrate was used for increasing its surface energy and 2-propanol (23 mN m^{-1}) was used as a cosolvent for decreasing the high surface tension of the water-based solution (72 mN m^{-1}). Preliminary tests showed that the 80:20 (wt:wt) mixture of water and 2-propanol, having a surface tension of about 30 mN m^{-1},[40,41] was the most suitable in terms of printability, in combination with an appropriate choice of the other process and ink parameters, as reported in the Experimental Section. In this regard, the viscosity is crucial; the prepared inks consist of a heterogeneous solid–liquid mixture containing polydispersed particles and the viscosity is strongly influenced by the interactions of particles with each other and with the solvent. Among the several physical parameters controlling such interactions, the main is the dispersed solid content.[42] For this reason,

preliminary tests have been conducted to find the highest solid fraction of ink having viscosity suitable for gravure printing that can allow a high quality of the printed layer. An ink having solid content of 14 wt% and viscosity of about 100 mPa s (measured on the previously ball-milled ink), resulting in a Ca value of 2, was found to generate the best print resolution. To reach an adequate mass loading for practical applications, a multilayer approach was adopted, printing consecutive layers on top of the previous ones, prior to the final drying (see **Table 1**).

A further challenge for the printed electrodes is related to the mix of the composites, which are made of materials with different particle sizes and different physicochemical properties. These components must be well dispersed in the ink as the functional proprieties of the final printed electrode strongly depend on the homogeneous distribution of all the components.

In a first attempt to produce printed anodes, the active material, the carbon additive, the binder, and the solvents were mixed by simple stirring. The resulting ink was printed on the copper substrate by overlapping seven printed layers. These electrodes showed good material distribution, while the secondary particles of the active material (with a diameter of around 10 μm) were still present, as revealed by the scanning electron microscopy (SEM) image (**Figure 2**). Nevertheless, half-cell tests of these electrodes, at constant and varying dis/charge rates, showed suitable specific capacities, very good rate capability, and good long-term cycling stability (**Figure 3**).

To increase the homogeneity of the layers and to decrease the size of the aggregates, the mixing process was improved. For this purpose, sonication and ball milling were used for the ink preparation either alone or in combination. **Figure 4** shows SEM images of the electrodes obtained by printing five layers of the inks prepared by different mixing methods. The sonication had a very low disaggregation effect, still showing the secondary aggregates of the active material (Figure 4a,a′). The ball-milled ink yields a more homogeneous printed layer with much smaller aggregates (Figure 4b,b′). The combination of sonication and ball milling slowly worsened the size homogeneity in the layer, probably due to partial reaggregation phenomena (Figure 4c,c′). The effect of the disaggregation techniques on the ink strongly influences the density of the final layer, as evident from the thickness (see Table 1). In fact, comparing the five-layer anodes, having same mass loading, the thickness of the only sonicated one is double that of the one of the ball-milled sample. The investigated batches using ball milling or sonication for the ink preparation showed long-term cyclability (>100 cycles) and comparable Coulombic efficiencies (Figure S1a, Supporting Information). However, the electrode made using the ball-milling step showed slightly higher capacities at high dis/charge rates (Figure S1b, Supporting Information). For these reasons, ball milling was adopted as the disaggregation technique for all the anodic inks' preparation. **Figure 5** shows the results of the five-layer gravure-printed electrodes following the ball-milling preparation. In fact, compared to the results shown in Figure 3 these electrodes showed slightly better rate capability, higher specific capacity with a high Coulombic efficiency, and enhanced cycling stability.

Table 1. Characteristics of the tested electrodes based on $Zn_{0.9}Fe_{0.1}O$–C as the active material.

Layer no.	Disaggregation technique	Overall active material [mg cm^{-2}]	Thickness of final layer [μm]
7	–	0.64 ± 0.09	20.0 ± 0.7
5	Sonication	0.55 ± 0.05	20.8 ± 0.4
5	Ball milling	0.55 ± 0.06	10.0 ± 0.7
5	Ball milling + sonication	0.49 ± 0.03	10.0 ± 0.7
10	Ball milling	1.32 ± 0.03	21.8 ± 1.5
15	Ball milling	1.72 ± 0.07	29.8 ± 2.8

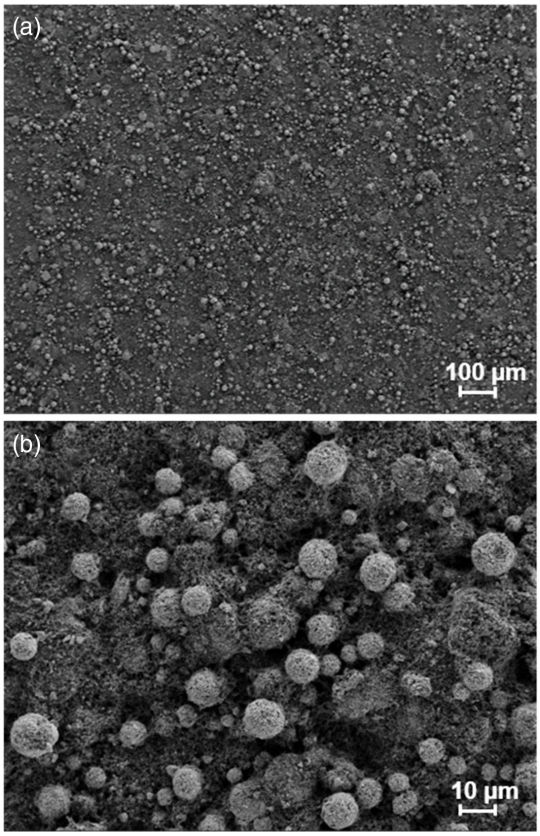

Figure 2. SEM images of the seven-layer gravure-printed electrode at a) low and b) high magnification.

Overlapping five layers, an active material mass loading of about 0.5 mg cm^{-2} was reached. Electrodes consisting of 10 and 15 printed layers were also made and investigated to enable the comparison of gravure-printed and tape-casted electrodes having similar mass loadings. The results show that the active material mass loading was, indeed, increased to about 1.3 mg cm^{-2} (10 layers) and 1.7 mg cm^{-2} (15 layers), respectively, with a very small standard deviation, supporting the high homogeneity of the printed layers (Table 1). Figure S2, Supporting Information, shows an SEM image of the cross-section of the 10-layer electrode, indicating that the particle distribution is homogeneous also in the bulk of the electrode printed layer. In **Figure 6**, the electrochemical characterization of the resulting electrodes via galvanostatic cycling is shown. The 10- and 15-layer electrodes show very similar Coulombic efficiencies and cycling

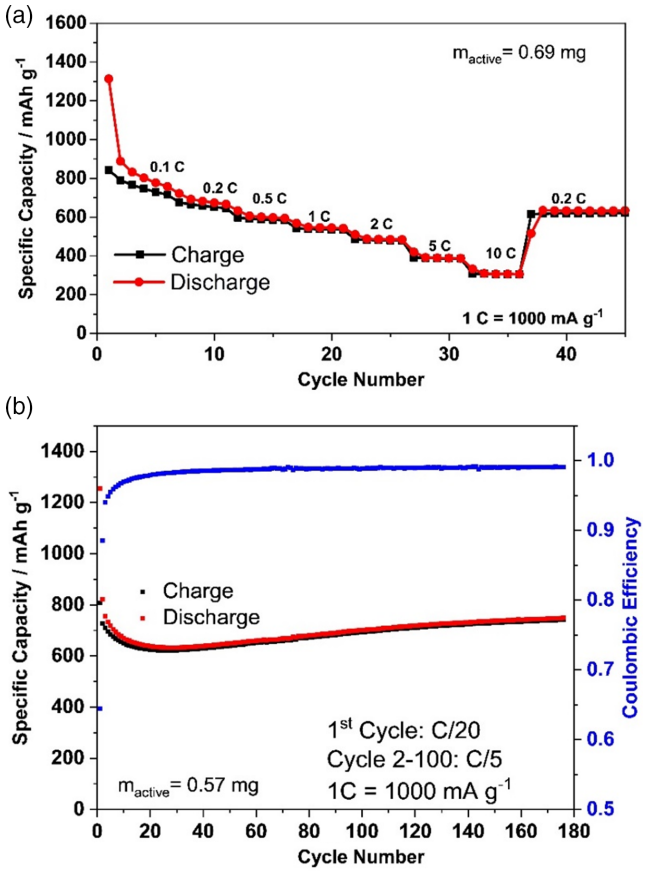

Figure 3. Plot of the specific capacity versus the cycle number of the seven-layer gravure-printed electrodes at a) increasing dis/charge rates and b) at a constant dis/charge rate of C/5 (first cycle at C/20; cutoff voltages: 0.01 and 3.0 V).

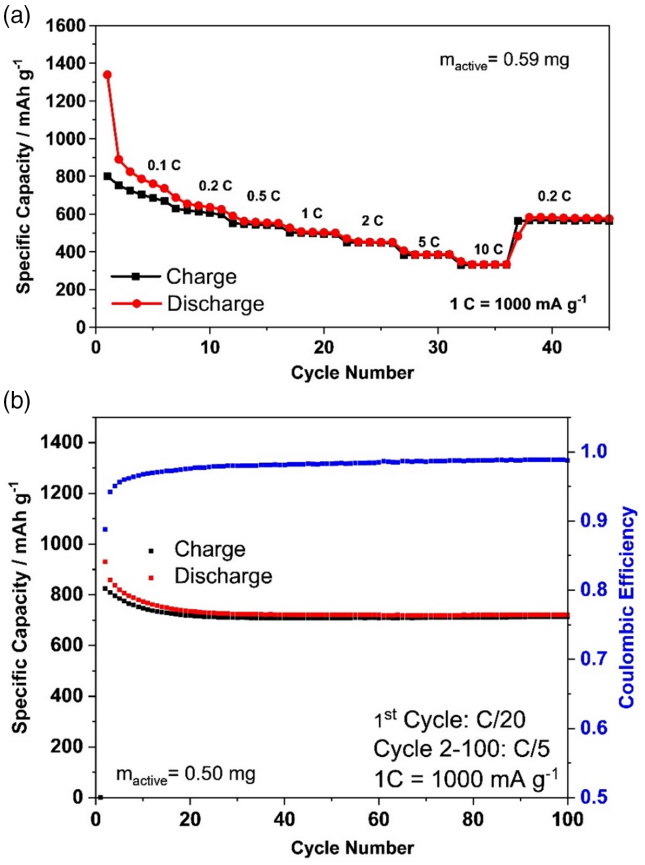

Figure 5. Plot of the specific capacity versus the cycle number of the five-layer gravure-printed electrodes using the ball-milling processing at a) increasing dis/charge rates and b) a constant dis/charge rate of C/5 (first cycle at C/20; cutoff voltages: 0.01 and 3.0 V).

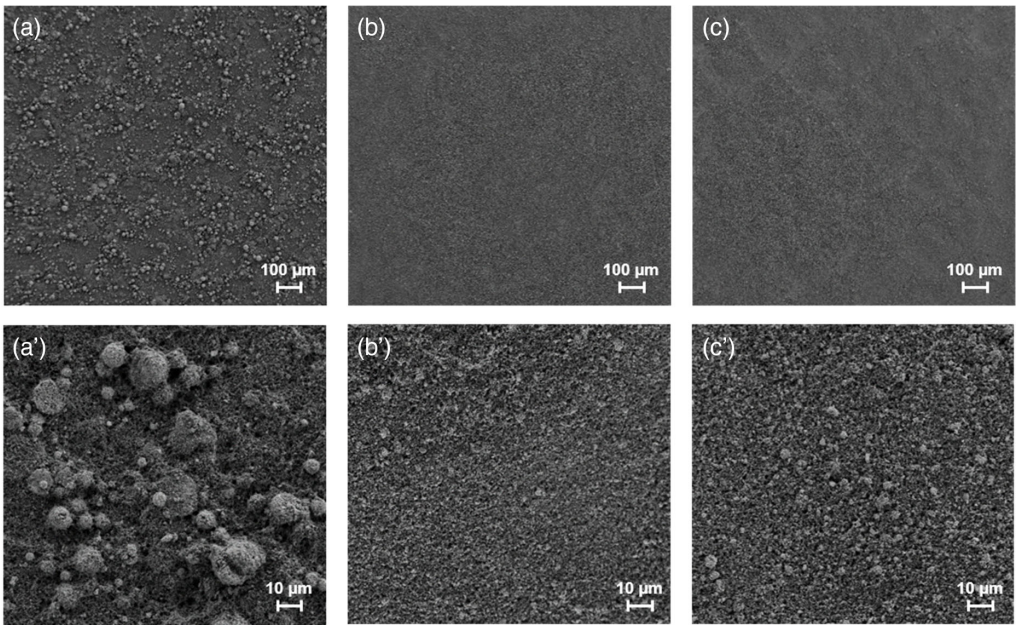

Figure 4. SEM images at two different magnifications of five-layer gravure printed electrodes prepared using a,a′) sonication, b,b′) ball milling, and c,c′) both techniques.

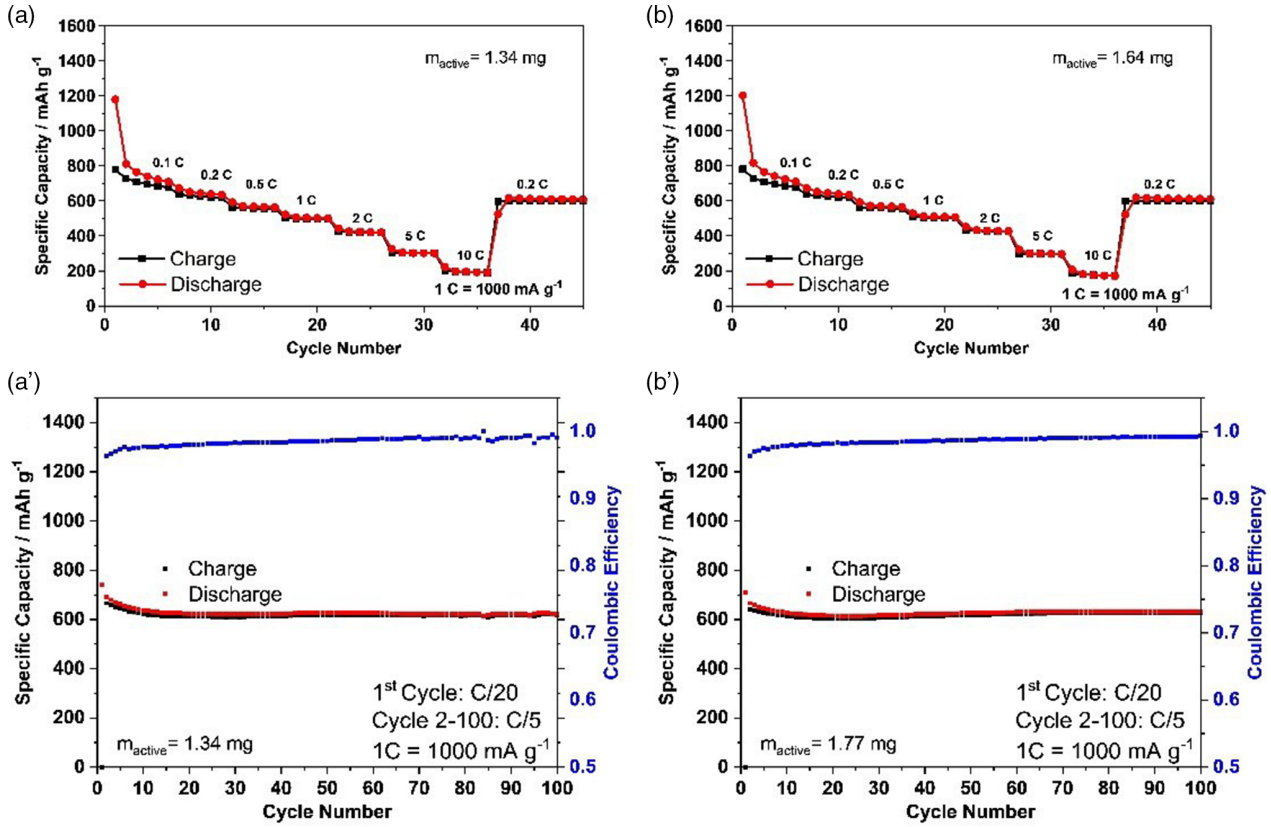

Figure 6. Plot of the specific capacity versus the cycle number of a,a′) the 10-layer gravure-printed electrodes and b,b′) the 15-layer gravure-printed electrodes at (a,b) increasing dis/charge rates and (a′,b′) a constant dis/charge rate of C/5 (first cycle at C/20; cut-off voltages: 0.01 and 3.0 V).

stability to those of the 5-layer electrodes and only slightly lower capacity; probably, in case of a high number of overlapped layers (≥10), at such fixed conditions of ink concentration and process parameters, a worsening of particle packing may occur. These confirm the efficacy of the gravure printing even for many overlapped layers and reasonable mass loadings (areal capacity of around 1 mAh cm^{-2}). To further highlight the suitability of this electrode fabrication process, the 10-layer gravure-printed electrodes were tested for 400 cycles with a limited upper cutoff voltage of 1.3 V (**Figure 7**), which represents a realistic voltage limit for the negative electrode in full Li-ion cells. The capacity remains excellently stable after the initial slight fading. This performance is in line with previous results achieved on doctor blade coating, which is the commonly used technique for electrode preparation.[26] It should be noted here that limiting the upper cutoff provides two positive effects regarding the application of such electrodes in LiBs. First, it has been shown that cycling $Zn_{0.9}Fe_{0.1}O$–C in a wide voltage window (i.e., between 0.01 and 3.0 V) leads to an unstable solid electrolyte interphase and, second, leads to a lower energy efficiency and density.[31,32,35] Consequently, such limitation to a narrower voltage range is beneficial for lithium-ion cells using such anodes if suitable prelithiation techniques are scaled up to the industrial level.[43]

The high cycling stability of the gravure-printed electrodes may be explained by the high homogeneity of the final gravure-printed electrodes. In general, the structure of the consolidated dried film depends on several parameters inherent to the contained particles (size, morphology, electrostatic charge, concentration), the rheology of the medium, and the drying conditions.[44] Inks (and slurries) are nonstabilized dispersions,

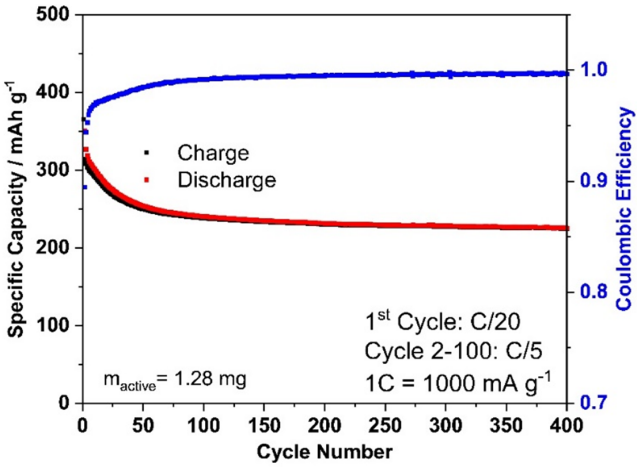

Figure 7. Plot of the specific capacity and Coulombic efficiency versus the cycle number of 10-layer gravure-printed electrodes cycled at C/5 (first cycle at C/20) with a limited upper cutoff voltage of 1.3 V.

consisting of heterogeneous particles of very different sizes. Accordingly, aggregation and sedimentation phenomena can occur.[45,46] In particular, the sedimentation cannot be neglected due to the size of the active material particles and the possibility of forming reaggregates, which are not in the colloidal range.[44,47] These phenomena can lead to a highly inhomogeneous final electrode, especially during drying, compromising its functional properties. Also, the drying is a very complex and dynamic process, coupling the bulk motion of the fluid and the particles' arrangement at the microscale, both strongly affecting the final film microstructure.[48] During the drying process, particulate layers tend to nonhomogeneously dry, leading to horizontal and vertical drying profiles and, thus, resulting in spatial inhomogeneity.[44,49] In particular, the vertical distribution results from the balance of diffusion and sedimentation during the evaporation. It is reasonable to assume that the smaller particles are in the evaporation regime, whereas the larger particles and aggregates are in the sedimentation-dominant regime.[44,46,48] These phenomena strongly encourage possible segregation in the drying layer, particularly across the thickness and especially when the dispersion is deposited in a single step with a large thickness (i.e., when performing tape casting, for instance). Such inhomogeneity is expected to play an important role for the charge transport pathways. The multilayer gravure printing may allow us to minimize such issues by better controlling the particle distribution, especially along the film thickness. In fact, in addition to the intrinsic high quality and reproducibility of the gravure printing process, using a multilayer process makes possible mitigation of the inhomogeneity along the overall thickness, generating a homogeneous microstructure of the composite anode. As the functional properties demonstrate, the reproducibility and quality of the gravure process allow us to potentially overlap any number of layers without affecting the properties of the final multilayer, thus being able to achieve the desired mass loadings.

Finally, it should be noted that the gravure-printed electrodes were not subjected to any postprocessing calendering. In this regard, it is useful to note that in case of microbatteries, such an additional step can be less important in increasing the volumetric density. In our case, the substantial reduction of the coating layer thickness by about 50% due to an optimization of the disaggregation technique (see Table 1) is certainly a key achievement, in combination with the described additional related advantages.

3. Conclusion

In this work, high-performance lithium-ion anodes based on $Zn_{0.9}Fe_{0.1}O$–C as the active material were successfully produced by gravure printing. Using the multilayer approach, electrodes with mass loadings ($>1.5\,mg\,cm^{-2}$), comparable to those commonly made by tape casting, were produced. It was proved that the gravure printing process allows us to potentially overlap any number of layers without affecting the properties of the final multilayer. These multilayer electrodes showed very good electrochemical performance in terms of achievable specific capacities, cycling stability, and rate capability. The long cycle life of the gravure-printed anodes is attributed to the high homogeneity of the printed layers, which allows very good distribution of the material components. Furthermore, the calendaring is skipped, maintaining the good electrochemical performance, making easier the overall production process. In this regard, the substantial reduction of the printed layer thickness by about 50% due to an optimization of the disaggregation technique is certainly a key achievement. The obtained results together with the use of environmentally-friendly materials promote the feasibility and sustainability of the well-established industrial gravure printing in the field of LiB production. In perspective, the use of only gravure printing as one-step production technique can be considered for the manufacturing of complete layered devices. Moreover, thanks to the high-quality film achieved, gravure printing appears as a useful tool in the study of new materials because of its capability to fully exploit the material characteristics.

4. Experimental Section

Materials: The materials used were as follows: microsized secondary particles of nanocrystalline $Zn_{0.9}Fe_{0.1}O$–C as the active material, sodium carboxymethyl cellulose (CMC) as binder (Dow Wolff Cellulosics), carbon black (Super C65, Imerys) as conductive carbon, 2-propaonl (Sigma Aldrich) as processing cosolvent, and Cu foil (Schlenk) as substrate. $Zn_{0.9}Fe_{0.1}O$–C was prepared via a recently reported scalable process including spray drying.[31] In brief, an aqueous solution of zinc(II) acetate dihydrate (Alfa Aesar) and iron(II) D-gluconate dihydrate (Aldrich) was spray dried (with a GEA Niro Mobile Minor spray dryer) and the resulting powder was calcined at 450 °C for 3 h (VMK-1400, Linn High Therm) and subsequently ball milled (Pulverisette 5, Fritsch). The resulting powder of $Zn_{0.9}Fe_{0.1}O$ nanoparticles was dispersed in an aqueous solution of β-lactose, spray dried, and then thermally treated at 500 °C for 4 h under an argon atmosphere (MK-135-S, Linn High Therm). Finally, the resulting $Zn_{0.9}Fe_{0.1}O$–C material was ground by planetary ball milling and granulated by spray drying.

Electrode Preparation: The electrode inks were prepared using 75 wt% of the active material, 19 wt% of carbon black, and 6 wt% of the CMC binder. A mixture of deionized water and 2-propanol (80:20 wt:wt) was used as solvent for the inks. Preliminary tests, changing the solid content of the ink (12–23 wt%), were conducted to find the best printable ink, with the used printing cylinder as reported subsequently. During the ink preparation process, the ink was sonicated for 1 h and/or ball milled for 3 h. The viscosity of the inks was measured by a viscosimeter (A&D SV-10) at 30 Hz constant frequency and 25 °C. The inks were deposited on Cu foils using a commercial lab-scale IGT G1-5 printer, equipped with a cylinder having a line density of 40 lines cm^{-1}, a stylus angle of 120°, a cell depth of 72 µm, and a screen angle of 53°. The Corona pretreatment was performed on a Cu foil to increase its surface energy ($<40\,mN\,m^{-1}$), improving its wettability.[50] To prevent possible sedimentation and flotation phenomena, the prepared dispersion was kept in slight agitation prior to printing. To produce thick films, a multilayer approach was adopted, overlapping layers of the same ink printed at the same conditions, simplifying the overall process: the wet ink was deposited on the previous layer, penetrating it and generating a unicum structure. After each layer printing, a fast drying was performed using nitrogen blow, while the overall anode was dried at 100 °C for 1 h. Different temperatures were tried to control the possible size-based particle segregation during the drying. In particular, the rate of evaporation was varied by changing the temperature from the ambient conditions up to 130 °C. High temperatures (>100 °C) were excluded as they caused curling of the substrate. A low evaporation rate was preferred for favoring the particle diffusion, thus avoiding possible stratification phenomena. The last stage at 100 °C was conducted to eliminate the residual water in the film. No final calendaring was applied on the printed anodes. Preliminary printing tests were conducted changing the printing speed and pressure, ranging from

12 to 60 m min^{-1} and 100 to 700 N, respectively, and were tried in different combinations; the best printing parameters were found to be a printing force of 700 N at a speed of 36 m min^{-1}. In Table 1, the characteristics of the prepared and tested electrodes are reported. Their morphology was investigated through SEM (Zeiss; LEO 1530). The electrode cross-section was investigated using a Zeiss Crossbeam 340 field-emission electron microscope, equipped with a Capella focused ion beam (FIB; with a gallium ion source).

Electrochemical Characterization: For the electrochemical tests, disk electrodes with a diameter of 12 mm were cut and dried for 12 h at 120 °C under vacuum. These electrodes were investigated in three-electrode Swagelok-type cells for evaluating the rate capability and in two-electrode coin cells for the long-term constant current cycling tests. All cells were assembled in an argon-filled glove box (MBraun, Germany) with an oxygen and water content below 0.1 ppm. A sheet of glass fiber fleece (Whatman, GFD), serving as separator, was drenched with 120 µL (150 µL for coin cells) of the electrolyte, consisting of 1 M $LiPF_6$ in a 3:7 (wt:wt) mixture of ethylene carbonate (EC) and diethyl carbonate (DEC). Lithium metal foils (Honjo) served as counter and reference electrodes. All provided capacities refer to the mass of the active material (including the carbon coating).

Supporting Information

Supporting Information is available from the Wiley Online Library or from the author.

Conflict of Interest

The authors declare no conflict of interest.

Data Availability Statement

Research data are not shared.

Keywords

anodes, conversion/alloying materials, gravure printing, lithium-ion batteries, multilayer approach, printed batteries

Received: April 20, 2021
Revised: June 10, 2021
Published online: July 16, 2021

[1] J. Oliveira, C. M. Costa, S. Lanceros-Méndez, in *Printed Batteries Materials, Technologies and Applications* (Eds: S. Lanceros-Méndez, C. M. Costa), John Wiley & Sons, Hoboken, NY **2018**.
[2] R. Gonçalves, J. Oliveira, M. P. Silva, P. Costa, L. Hilliou, M. M. Silva, C. M. Costa, S. Lanceros-Méndez, *ACS Appl. Energy Mater.* **2018**, *1*, 3331.
[3] P. Rassek, E. Steiner, M. Herrenbauer, T. C. Claypole, *Flexible Printed Electron.* **2019**, *4*, 035003.
[4] P. Rassek, E. Steiner, *Appl. Phys. A* **2020**, *126*, 741.
[5] R. Gonçalves, P. Dias, L. Hilliou, P. Costa, M. M. Silva, C. M. Costa, S. Corona-Galván, S. Lanceros-Méndez, *Energy Technol.* **2021**, *9*, 2000805.
[6] J. Wang, Q. Sun, X. Gao, C. Wang, W. Li, F. B. Holness, M. Zheng, R. Li, A. D. Price, X. Sun, T.-K. Sham, X. Sun, *ACS Appl. Mater. Interfaces* **2018**, *10*, 39794.
[7] X. Gao, Q. Sun, X. Yang, J. Liang, A. Koo, W. Li, J. Liang, J. Wang, R. Li, F. B. Holness, A. D. Price, S. Yang, T.-K. Sham, X. Sun, *Nano Energy* **2019**, *56*, 595.
[8] X. Lin, J. Wang, X. Gao, S. Wang, Q. Sun, J. Luo, C. Zhao, Y. Zhao, X. Yang, C. Wang, R. Li, X. Sun, *Chem. Mater.* **2020**, *32*, 3018.
[9] C. M. Costa, R. Gonçalves, S. Lanceros-Méndez, *Energy Storage Mater.* **2020**, *28*, 216.
[10] G. Grau, J. Cen, H. Kang, R. Kitsomboonloha, W. J. Scheideler, V. Subramanian, *Flexible Printed Electron.* **2016**, *1*, 023002.
[11] G. Grau, V. Subramanian, *Flexible Printed Electron.* **2020**, *5*, 014013.
[12] R. R. Søndergaard, M. Hösel, F. C. Krebs, *J. Polym. Sci. Part B Polym. Phys.* **2013**, *51*, 16.
[13] J. Puetz, M. A. Aegerter, *Thin Solid Films* **2008**, *516*, 4495.
[14] D. A. Alsaid, E. Rebrosova, M. Joyce, M. Rebros, M. Atashbar, B. Bazuin, *J. Disp. Technol.* **2012**, *8*, 391.
[15] S. Khan, L. Lorenzelli, R. S. Dahiya, *IEEE Sens. J.* **2015**, *15*, 3164.
[16] Q. Huang, Y. Zhu, *Adv. Mater. Technol.* **2019**, *4*, 1800546.
[17] Z. Liu, P. P. Mukherjee, *J. Electrochem. Soc.* **2014**, *161*, E3248.
[18] J. Liu, B. Ludwig, Y. Liu, Z. Zheng, F. Wang, M. Tang, J. Wang, J. Wang, H. Pan, Y. Wang, *Adv. Mater. Technol.* **2017**, *2*, 1700106.
[19] A. Varzi, K. Thanner, R. Scipioni, D. Di Lecce, J. Hassoun, S.ne. Dörfler, H. Altheus, S. Kaskel, C. Prehal, S. A. Freunberger, *J. Power Sources* **2020**, *480*, 228803.
[20] M. Montanino, A. De Girolamo Del Mauro, M. Tesoro, R. Ricciardi, R. Diana, P. Morvillo, G. Nobile, A. Imparato, G. Sico, C. Minarini, *Polym. Compos.* **2015**, *36*, 1104.
[21] G. Sico, M. Montanino, A. De Girolamo Del Mauro, A. Imparato, G. Nobile, C. Minarini, *Org. Electron.* **2016**, *28*, 257.
[22] M. Montanino, G. Sico, C. T. Prontera, A. De Girolamo Del Mauro, S. Aprano, M. G. Maglione, C. Minarini, *eXPRESS Polym. Lett.* **2017**, *11*, 518.
[23] G. Sico, M. Montanino, A. De Girolamo Del Mauro, C. Minarini, *J. Mater. Sci. Mater. Electron.* **2018**, *29*, 11730.
[24] G. Sico, M. Montanino, C. T. Prontera, A. De Girolamo Del Mauro, C. Minarini, *Ceram. Int.* **2018**, *44*, 19526.
[25] M. Montanino, G. Sico, A. De Girolamo Del Mauro, M. Moreno, *Membranes* **2019**, *9*, 71.
[26] D. Bresser, F. Mueller, M. Fiedler, S. Krueger, R. Kloepsch, D. Baither, M. Winter, E. Paillard, S. Passerini, *Chem. Mater.* **2013**, *25,* 4977.
[27] D. Bresser, S. Passerini, B. Scrosati, *Energy Environ. Sci.* **2016**, *9*, 3348.
[28] J. Cabana, L. Monconduit, D. Larcher, M. R. Palacín, *Adv. Mater.* **2010**, *22*, E170.
[29] M. N. Obrovac, V. L. Chevrier, *Chem. Rev.* **2014**, *114*, 11444.
[30] J. Lu, Z. Chen, F. Pan, Y. Cui, K. Amine, *Electrochem. Energy Rev.* **2018**, *1*, 35.
[31] J. Asenbauer, J. R. Binder, F. Mueller, M. Kuenzel, D. Geiger, U. Kaiser, S. Passerini, D. Bresser, *ChemSusChem* **2020**, *13*, 3504.
[32] J. Asenbauer, A. Varzi, S. Passerini, D. Bresser, *J. Power Sources* **2020**, *473*, 228583.
[33] A. Gören, J. Mendes, H. M. Rodrigues, R. E. Sousa, J. Oliveira, L. Hilliou, C. M. Costa, M. M. Silva, S. Lanceros-Méndez, *J. Power Sources* **2016**, *334*, 65.
[34] C. M. Costa, H. M. Rodrigues, A. Gören, A. V. Machado, M. M. Silva, S. Lanceros-Méndez, *ChemistrySelect* **2017**, *2*, 5394.
[35] J. Asenbauer, A. Hoefling, S. Indris, J. Tübke, S. Passerini, D. Bresser, *ACS Appl. Mater. Interfaces* **2020**, *12*, 8206.
[36] F. C. Krebs, *Sol. Energy Mater. Sol. Cells* **2009**, *93*, 394.
[37] Y. Choi, G. H. Kim, W. H. Jeong, H. J. Kim, B. D. Chin, J.-W. Yu, *Thin Solid Films* **2010**, *518*, 6249.
[38] S. S. Hwang, C. G. Cho, K.-S. Park, *Electrochem. Commun.* **2011**, *13*, 279.
[39] P. Rassek, M. Wendler, M. Krebs, in *Printed Batteries Materials, Technologies and Applications* (Eds: S. Lanceros-Méndez, C. M. Costa), John Wiley & Sons, Hoboken, NY **2018**; Ch. 7.

[40] H. Ghahremani, A. Moradi, J. Abedini-Torghabeh, S. M. Hassani, *Chem. Sin.* **2011**, *2*, 212.
[41] F. Biscay, A. Ghoufi, P. Malfreyt, *J. Chem. Phys.* **2011**, *134*, 044709.
[42] M. Briceno, *in Pharmaceutical Emulsions and Suspensions* (Eds: F. Nielloud, G. Marti-Mestres), CRC Press, Boca Raton, FL **2000**.
[43] F. Holtstiege, P. Bärmann, R. Nölle, M. Winter, T. Placke, *Batteries* **2018**, *4*, 4.
[44] O. Cusola, S. Kivistö, S. Vierros, P. Batys, M. Ago, B. L. Tardy, L. G. Greca, M. B. Roncero, M. Sammalkorpi, O. J. Rojas, *Langmuir*, **2018**, *34*, 5759.
[45] S. Vesaratchanon, A. Nikolov, D. T. Wasan, *Adv. Colloid Interface Sci.* **2007**, *134–135*, 268.
[46] P. Aimar, P. Bacchin, in *Nano-Science: Colloidal and Interfacial Aspect* (Ed: V. M. Starov), CRC Press, Boca Raton, FL **2010**.
[47] M. Schulz, J. L. Keddie, *Soft Matter* **2018**, *14*, 6181.
[48] M. Wang, J. F. Brady, *Soft Matter* **2017**, *13*, 8156.
[49] R. E. Trueman, E. Lago DominguesDomingues, S. N. Emmett, M. W. Murray, A. F. Routh, *J. Colloid Interface Sci.* **2012**, *377*, 207.
[50] N. Billot, T. Günther, D. Schreiner, R. Stahl, J. Kranner, M. Beyer, G. Reinhart, *Energy Technol.* **2020**, *8*, 1801136.